Results in Physics 12 (2019) 2146–2154

Contents lists available at ScienceDirect

Results in Physics

journal homepage: www.elsevier.com/locate/rinp

The field-dependent rheological properties of plate-like carbonyl iron particle-based magnetorheological elastomers

Norhiwani Hapipi[a], Siti Aishah Abdul Aziz[a], Saiful Amri Mazlan[a,*], Ubaidillah[b,c,*], Seung Bok Choi[d,*], Norzilawati Mohamad[a], Muntaz Hana Ahmad Khairi[a], Abdul Yasser Abd. Fatah[e]

[a] AVS Research Laboratory, Malaysia-Japan International Institute of Technology (MJIIT) Universiti Teknologi Malaysia, Jalan Sultan Yahya Petra, 54100 Kuala Lumpur, Malaysia
[b] Mechanical Engineering Department, Faculty of Engineering, Universitas Sebelas Maret, Jl. Ir. Sutami 36A, Kentingan, Surakarta 57126, Central Java, Indonesia
[c] National Center for Sustainable Transportation (NCSTT), Bandung, Indonesia
[d] Department of Mechanical Engineering, Inha University, 253, Yonghyun-dong, Namgu, Incheon 402-751, South Korea
[e] Department of Engineering, Razak School of Engineering and Advanced Technology, Universiti Teknologi Malaysia, Jalan Sultan Yahya Petra, 54100 Kuala Lumpur Malaysia

A B S T R A C T

This paper investigated the rheological properties of a novel magnetorheological elastomer (MRE) with plate-like carbonyl iron particles (CIPs) as magnetic particles. MRE samples with different shape of CIPs; plate-like (MRE-P) and spherical-like (MRE-S), were prepared. The current work further highlights the effects of varying curing magnetic field towards the rheological properties. X-ray diffraction and magnetic properties analysis were carried out to observe not only the surface morphology of the CIPs but also the cross-section of CIPs in the MRE samples. Rheological properties such as strain amplitude, frequency, and magnetic field sweep test were measured using a rotational rheometer. The MRE-P samples demonstrated higher storage modulus and the loss factor lower than MRE-S. Besides that, the MR effect of MRE-P samples is slightly lower than that of MRE-S correspond to 114% and 137%, respectively.

Introduction

Magnetorheological elastomer (MRE) is a type of smart materials, where the rheological properties can be changed by controlling the external magnetic field and exhibited through its magnetic field-dependent modulus and damping properties. These unique properties of MRE are mainly attributed to the micron-sized magnetic particles that had been embedded in the elastomer or rubbery-like matrix materials. Under the influences of magnetic fields, the inter-particle forces between the magnetic particles inside the matrix are then generated to produce magnetized particles [1,2]. As a result, chain-like structures that restrict rubber deformation and slippage are formed, hence causing the changes of the modulus [3]. Apart from the changes of storage modulus, the MR effect [4] can also be demonstrated through the changes in the loss modulus as well as the damping factor, which had become a key parameter in the evaluation of MRE performance [5–7]. With its controllable properties, this has allowed MRE to be used in a broad range of engineering field applications such as absorbers [8,9,10,11], dampers [12,13] and sensors [14,15].

In the recent decades, most studies had not only focused on the types of matrix and magnetic particles, but also on particle orientations and particle volume fractions [16–18]. Technically, although the conventional spherical Carbonyl Iron Particle (CIP) is the most commonly used magnetic particles in MRE fabrication, its overemphasis and the lack of discussions conducted on the particle-shaped CIPs had thus neglected the possible influence of the latter on the rheological properties of MRE [19,20]. Nevertheless, several studies had introduced the importance of plate-like, PL CIPs in solving the existing sedimentation issue in certain MR materials such as MR fluid (MRF) and MR grease (MRG) [21,22], where the flaky or PL-shaped particles were found to have exhibited greater yield stress and higher stability as a result of the increased surface energy in the particles. In their investigations on the field-dependent rheological properties of the PL-based CIPs MRF, Shah et al. [23,24] and Shilan et al. [25] had found the introduction of the PL CIPs to not only reduced the sedimentation issues, but had also enhanced the particles stability as well as the magnetic saturation of the MRF. Meanwhile, in fabricating the MRG with a different weight ratio of PL CIPs, Mohamad et al. [26] had discovered the larger surface contact areas of the PL CIPs to have contributed to a highly viscous and more elastic MRG at lower fractions.

* Corresponding authors at: Mechanical Engineering Department, Faculty of Engineering, Universitas Sebelas Maret, Jl. Ir. Sutami 36A, Kentingan, Surakarta 57126, Central Java, Indonesia (Ubaidillah).
E-mail addresses: amri.kl@utm.my (S.A. Mazlan), ubaidillah_ft@staff.uns.ac.id (Ubaidillah).

https://doi.org/10.1016/j.rinp.2019.02.045
Received 24 December 2018; Received in revised form 14 February 2019; Accepted 14 February 2019
Available online 19 February 2019

Many of the studies conducted on the PL CIPs in MREs however, had only focused on its electromagnetic absorbing property [19,27–29]. Since the PL CIPs had demonstrated an easy magnetization axis and smaller demagnetization factor that effectively exceed the Snoek limit, the material was deemed suited for military and civil applications, such as stealth coating and the absorbing patches found on mobile phones [27,28]. This was not only attested by Zhenjiang et al. [29], who had reported the larger aspect ratio and higher value of magnetic permeability and permittivity achieved by PL CIPs in reducing the eddy current loss to be one of the best candidates for microwaveable absorption materials, but also by Kumar et al., who had discovered the rod-like CIPs particles having a higher storage modulus as a result of its better stress transferability [19]. Despite using the results derived from microwave studies, the PL CIPs can still be regarded as providing a better MR effect just by solely referring to the findings of the rod-shaped particles on the MRE. To the best of the authors' knowledge, since there had been no systematic studies conducted on the rheological properties of MREs incorporated with PL CIPs as magnetic particles, a thorough study on the rheological properties of the PL MRE towards the existence of external magnetic field would be an interesting area to delve in as this would involve analyzing the effects of magnetic field strength on the PL CIP-based MRE during curing process under strain amplitude, frequency and current sweep of testing parameters. In this study, the investigation on the effect of curing conditions towards the rheological properties had involved the incorporation of two different shapes of CIPs in the MREs, namely the MRE-S and MRE-P samples, which had been fabricated and prepared under isotropic and anisotropic conditions. Apart from using the rheological test as a means of comparing both the MRE-S and MRE-P properties, a scanning electron microscopy (SEM), X-ray diffraction (XRD) and mapping methods were also carried out to confirm the morphology of the PL CIPs and MRE samples.

Experimental setup

Raw materials

Soft magnetic carbonyl iron particles (CIP: type OM, d_0 = 1–10 μm) were supplied by BASF Corporation, Germany. Room-temperature-vulcanized silicone rubber (RTV-SR) were purchased from Nippon Steel (NS625). Peroxide liquid was used as the curing agent.

Preparation of PL CIPs

In this study, SL-CIPs were milled using a rotary (QM-5 model form Tencan Company) to alter the shapes. The zirconia balls were used as the grinding media and the ball-to-powder ration is set to 20:1. The SL-CIPs were milled with 380 rpm for 40 h to obtain PL-CIPs. In addition, pure ethanol was added as the control agent to avoid particles adhesion and to improve the efficiency in producing plate-like particles [25].

Fabrication of Si-rubber based MRE samples

Firstly, the silicone-based MRE samples were prepared by mixing 70 wt% of CIPs with the silicone rubber liquid, and the mixture was stirred vigorously for about 10 min to ensure the homogeneity. Then, the curing agent was added into the silicone matrix with the weight ratio of 100:2 and stirred again for 2 min as suggested by the manufacturer. Finally, the mixture was poured into a customized mold with a thickness of 1 mm. The MRE sample was left to cure at ambient temperature for 2 h before released from the mold. Two different types of MRE which are isotropic and anisotropic were prepared without and with the external magnetic field, respectively. The anisotropic MRE was cured in the presence of magnetic field varied from 70, 209, and 345 mT. The schematic diagram of the fabrication process is shown in Fig. 1. Two groups of MRE samples (MRE-P and MRE-S) were prepared with different shapes of CIPs which are PL-CIPs and SL-CIPs, respectively. The detailed compositions of the MRE samples for each group are shown in Table 1.

Characterizations

The surface morphology of the CIPs and the cross-section of the MRE samples were observed using a scanning electron microscope (SEM, JEOL-IT300). The test was conducted with the application of an accelerating voltage of 6 kV with the magnification of 4000× for the surface morphology. The mean particles size distribution of the magnetic particles was determined using particle size analyzer (PSA). For the cross-section of MRE, the accelerating voltage and magnification were 15 kV and 1000× respectively. The crystalline structure analysis of the SL-CIPs and PL-CIPs was carried out by X-ray diffraction (Empyrean, PANalytical) while the magnetic properties were examined using vibrating sample magnetometer (VSM, MIcrosense 7404). The dynamic mechanical properties of the MRE samples were measured by using a rheometer (Model: MCR 302 Anton Paar). Three types of testing were done to measure the dynamic properties of the samples which are shear storage modulus, loss factor, and MR effect. The dynamic testing conditions for rheological properties were listed as follows:

Strain amplitude sweep testing: The frequency was set at 1 Hz, and the testing magnetic field strengths were fixed at 0 (off-state) and 600 mT (on-state). The strain was swept from 0.001 to 20%.

Magnetic field sweep testing: The shear strain amplitude and frequency were fixed at 0.02%, and 1 Hz, respectively. The magnetic field was swept from 0 to 800 mT.

Excitation frequency sweep testing: The shear strain amplitude was set at 0.02%, meanwhile, the testing magnetic fields were fixed at 0 (off-state) and 600 mT (on-state). The frequency was swept from 0.1 to 100 Hz.

Results and Discussions in Morphological Aspect

Morphology of PL CIPs

The SEM images of SL CIPs and PL CIPs are shown in Fig. 2, while Fig. 3 shows their particle size distribution. Fig. 2(a) shows the unmilled CIPs or the SL-CIPs with initial spherical shapes and average size distribution of ~3 μm. Meanwhile, in Fig. 2(b), the particle morphology of the CIPs had transformed from one of SL to a PL structure, where the CIPs had flattened with an averagely increased size distribution of up to 5 μm. In Fig. 3, the thickness of the milled CIPs had also reduced with a wider diameter, which had agreed well with the previous study conducted by Shilan et al. [25]. The particle size distribution of the SL and PL CIPs were measured by using the Laser Diffraction Particle Size Analyzer SALD-2300. As depicted in Fig. 3, the graph had clearly shown the SL CIPs having an average mean diameter of 5 μm, while the average mean diameter of PL CIPs had been larger at about 6 μm as a result of being flattened during the milling process.

Phase characterization

The XRD patterns of the two different types of CIPs are illustrated in Fig. 4. It could be observed that both of the SL-CIPs and PL-CIPs had exhibited two broad peaks at 44.72° and 65.67° that had corresponded to the (1 1 0) and (2 0 0) planes in 2θ and correlated to the peaks of α-Fe. These two intense peaks at 44.72° and 65.67° had been very sharp, thus indicating a well-defined crystallized structure of the CIPs. The XRD patterns had therefore confirmed the crystallized structure of SL-CIPs and PL-CIPs to be of a body-centered cubic (bcc) phase, which had agreed well with the findings conducted by other researchers [28,29]. Although the results had shown no emergence of new and different peaks with changes in the CIP shape, the intensity peaks of SL-CIPs however, had been slightly higher than those of PL-CIPs. There were

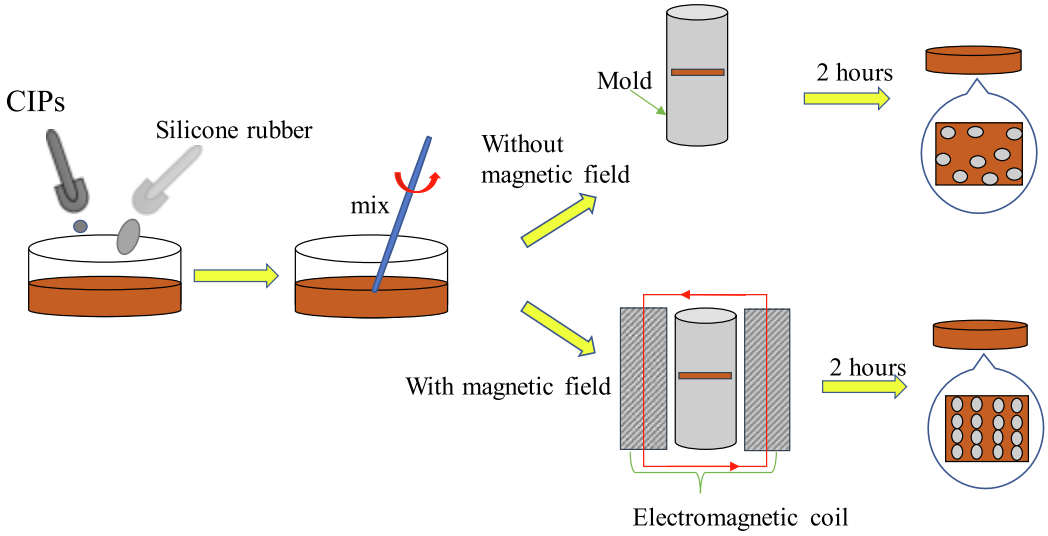

Fig. 1. A schematic diagram of the fabrication process of MRE.

Table 1
Compositions of the MRE samples.

	Sample no.	SL CIP (wt.%)	PL CIP (wt.%)	Silicone rubber (wt.%)	Curing condition (magnetic field, mT)
1	MRE-S1	70	–	30	0
2	MRE-S2	70	–	30	70
3	MRE-S3	70	–	30	209
4	MRE-S4	70	–	30	345
5	MRE-P1	–	70	30	0
6	MRE-P2	–	70	30	70
7	MRE-P3	–	70	30	209
8	MRE-P4	–	70	30	345

also no peaks related to impurities as shown by the non-appearance of other phases. Hence, it can be concluded that the milling process had not changed the structural characterization of the CIPs.

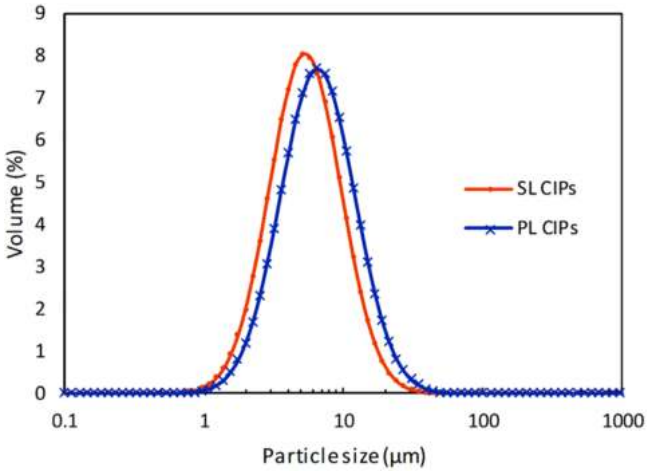

Fig. 3. Particle size distributions of SL CIPs and PL CIPs.

The magnetic property of CIPs

Fig. 5 illustrates the magnetic hysteresis loops of both SL CIPs and PL CIPs, while Table 2 presents the important magnetic parameters that had been extracted from Fig. 5. Based on the hysteresis loop curves shown in Fig. 5, the saturation magnetization of M_s of SL CIPs and PL CIPs were shown to have a respective value of 143.79 and 141.59 emu/g (Table 2). The lower value of Ms for PL CIPs is referred to as the movement of particles, where the PL CIPs had reached Ms more easily than the SL CIPs because of the higher static permeability [28,30]. As stated by Bell et al. [31], the magnetic saturation had depended on the size, shape, and dimension of the particles. However, the PL CIPs had exhibited a higher coercive force of 22.99 Oe than the 12.38 Oe

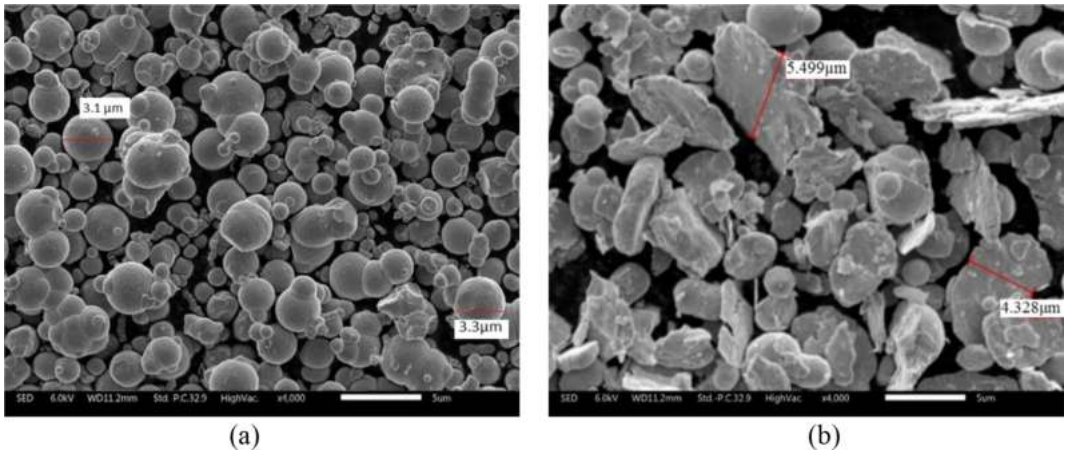

Fig. 2. SEM images of CIPs (a) SL-CIPs and (b) PL-CIPs.

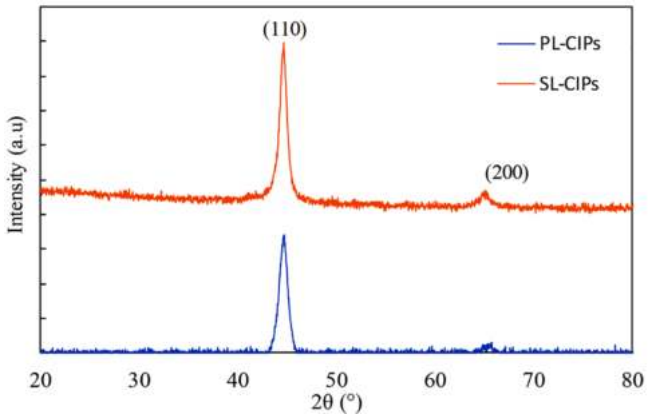

Fig. 4. XRD patterns analysis of the SL CIPs and PL CIPs.

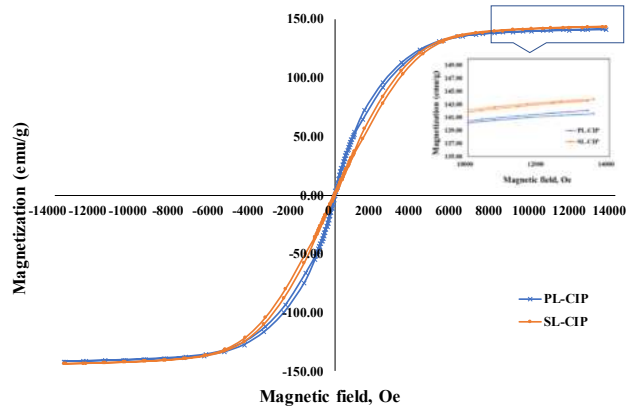

Fig. 5. Magnetic hysteresis loops of SL CIPs and PL CIPs.

Table 2
Magnetic properties of different shapes of CIPs.

Samples/parameters	SL CIP	PL CIP
M_s (emu/g)	143.79	141.59
M_r (emu/g)	0.4611	1.7303
H_c (Oe)	12.377	22.987

exhibited by SL CIPs. This is due to the enhanced shape anisotropy of the PL CIPs, where in theory, is one of the major driving mechanisms for coercivity. In this case, particles with smaller demagnetization factor in the longest direction are seen to possess larger coercivities, hence supporting the findings from other previous researchers [28,32] such as those by Qiao et al. [32], who had stated the higher coercive forces that were attributed to the increase of the pinning domain walls as being possibly related to the introduction of shape anisotropy in the PL CIPs.

Morphology of MRE samples

The SEM images of the cross-section morphologies of the MRE-S and MRE-P, isotropic (0 mT) and anisotropic (345 mT) are shown in Fig. 6, where the CIPs had been observed to be well-embedded and distributed in the matrix. The bright and white parts had represented the CIPs, while the black and dark parts were the silicon rubber. As shown in Fig. 6(a), the CIPs were randomly distributed in the silicone-matrix with some agglomeration observed in the MRE samples, while in Fig. 6(b), the CIPs had formed chain-like structures that were aligned according to the magnetic field direction. This formation of chain-like structures could have occurred because of the external magnetic field that had existed during the curing process [33]. Under an anisotropic orientation, the agglomeration between the particles had become smaller as a result of the interaction forces between the particles. As mentioned by Li et al. [34], the number of distance between the particles is significant for ensuring flow uniformity as well as in reducing the interfacial area between the particles and the matrix. Meanwhile, Fig. 6(c) and (d) shows the SEM image of the cross-sectional morphology of the isotropic and anisotropic structured MRE-P samples, respectively. The results from Fig. 6(c) had revealed the PL CIPs filling up the void of the silicone matrix as well as the reduced gaps between the particles and rubber that were caused by the wider distribution of the PL-CIPs. Concurrently, the small agglomerations that were observed in the MRE samples with PL-CIPs as a result of the larger particles diameter had also made the samples floppy, hence affecting the final performance of the MRE samples [35]. Furthermore, as shown in Fig. 6(d), PL-CIPs in anisotropic orientation tend to form chain-like structures, edge-to-edge of the particles and formed structures like “house of cards”. The formations of “house of cards” structures of PL-CIPs, proved that the anisotropy shape anisotropy of PL-CIPs magnetize more easily along the long axis of the particles depending on the direction of magnetic field. Whereas, in isotropic orientation shown in Fig. 6(c), the PL-CIPs are randomly distributed in several ways: face to face, edge to face or edge to edge because the particles not influenced by any direction of external magnetic field.

Results and discussions in rheological aspect

Strain amplitude sweep test

The strain amplitude sweep test was carried out to investigate the effect of shear strain on the dynamic viscoelastic modulus of the MRE samples. This mechanism had applied a fixed oscillatory strain on the specimen and had involved the measurement of amplitude and phase of the output force in the calculation of the shear storage modulus. The strain amplitude sweep test was carried out by varying the strain from 0.001 to 20% with a constant frequency of 1 Hz in a typical room temperature of 25 °C. Fig. 7 shows the storage modulus of the MRE samples as a function of the strain amplitude.

As depicted in Fig. 7(a), all of the MRE samples had exhibited strain-dependent behavior, where the shear storage modulus, G’ had decreased with increasing strain amplitude. In isotropic samples, however, only a slight decrease of G’ was observed for MRE-S1 and MRE-P1. This phenomenon had therefore indicated a typical Payne effect behavior for filled elastomer, where it denotes the dependency of storage modulus on strain amplitudes that were caused by the destruction and reformation of a magnetic particle network. In Fig. 7(b), since the physical mechanism of the Payne effect is mostly related to the destruction and reformation of a magnetic particle network in the presence of a magnetic field, the Payne effect had been more pronounced when performed during an on-state condition. The bonding between rubber-fillers will result in an increased network density of the MRE samples as each of the stable or unstable bonds could give rise to either an increment or decrement of network density.

Theoretically, this network density is supposed to vary with the deformation of MRE materials, where the unstable bonds will most likely break with applied mechanical stress. This phenomenon will then result in the breakdown of filler networks, hence releasing the entrapped elastomer that decreases the shear storage modulus. The effect of strain amplitude on G’ for different curing magnetic fields and particle shapes is shown in Table 3. As seen from the table, the strain amplitude on all of the samples had increased steadily with increasing curing magnetic fields until a saturated level is reached for both the MRE-S and MRE-P samples. The increases of G’ had been due to the generated restrained rubber that had formed as a result of the triggered magnetic particles movement during the curing process, which contributing factor of a higher modulus. Furthermore, the application of a

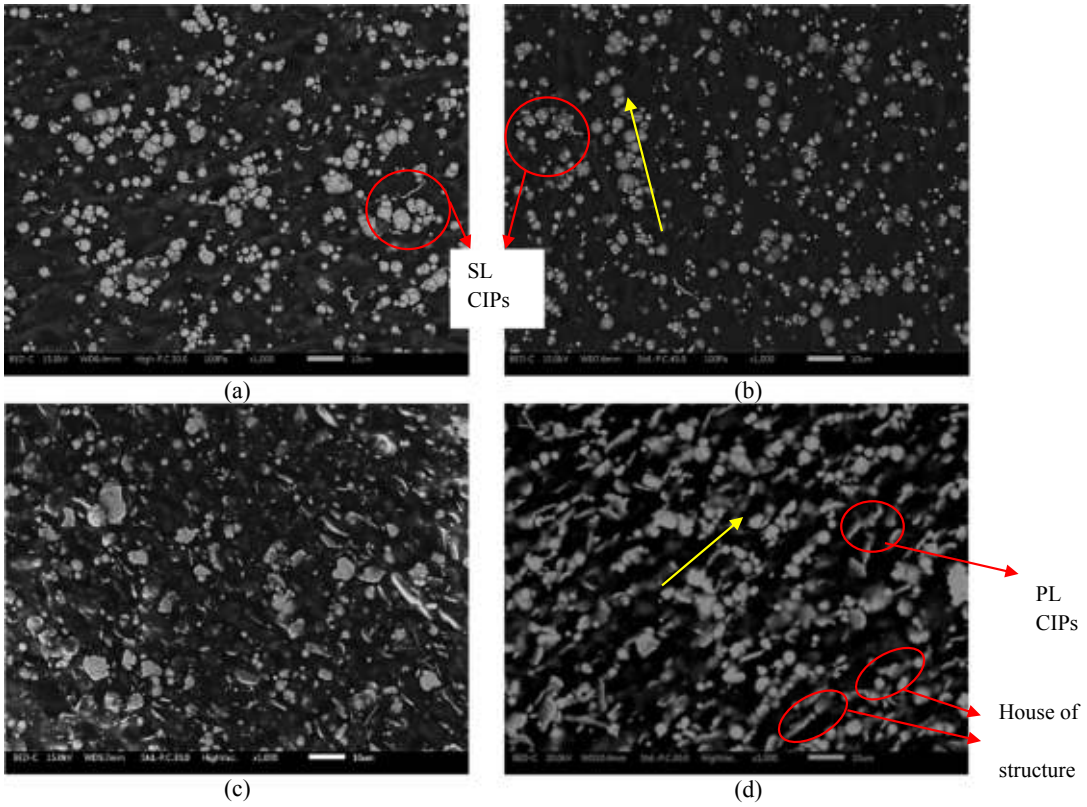

Fig. 6. SEM images of (a) isotropic for MRE-S, (b) anisotropic structured for MRE-S (c) isotropic structured for MRE-P and (d) anisotropic structured for MRE-P with 70 wt%.

stronger magnetic field on the prepared samples had also led to a higher occurrence of more restrained rubber. The initial, maximum, as well as the magneto-induced moduli of the samples, are summarized accordingly in Table 3.

From Table 3, the value of the MRE-P initial modulus was observed to be higher than those of MRE-S samples at off-state condition and had shown a continuous increasing trend with increasing curing magnetic fields. Since stiffer material is known to lead to a harder deformation of the MRE samples, the higher value of G_0 for the MRE-P samples had been due to the increased stiffness of the rubber materials, which were caused by the diameter and thickness changes of the PL CIPs during the deformation of MRE samples. Meanwhile in the on-state condition, the presence of a magnetic field had strongly influenced the behavior of MRE, particularly the MRE-P samples. As shown in Table 3, although the G_0 values for the respective MRE-P and MRE-S samples had increased with increasing curing magnetic fields, the G_0 value for the anisotropic MRE-P samples however, had been slightly lower than those of the anisotropic MRE-S samples. This phenomenon could be explained by not only due the low magnetic saturation and high coercivity force of PL CIPs, but also the larger surface of PL CIPs in MRE-P. The results agreed well with the morphological properties observed in Fig. 6(d) in which at on-state condition, the MRE with PL-CIPs tend to align following the direction of magnetic field, and form “house of card” structures. Those chain structures are weak since they are attracted like the edge-to-edge and easily to break at higher strains during oscillatory test.

Frequency sweep test

Since MREs are commonly employed in vibration and acoustic devices, it is therefore necessary to apply the frequency excitation sweep test as a way of evaluating its dynamic stiffness and damping properties. These frequency sweeps had been performed in a range of 0.1–100 Hz with a constant strain amplitude of 0.02% (within the LVE region), while the storage modulus and loss factor were recorded as a function of the frequency level. The storage modulus of MRE as a function of the frequency level at both off- and on-state conditions are depicted in Fig. 8.

As shown in Fig. 8, the G’ for samples MRE-S and MRE-P had gradually increased with increasing driving frequencies at both off- and on-state conditions. In viscoelastic materials, it is a common phenomenon that frequency intensities will lead to increased entanglements in the matrix, since the deformation of molecule chains had failed to keep up with the shear force, hence causing the G’ to increase with increasing frequency intensities [36]. The G’ of the isotropic samples (MRE-P1 and MRE-S1) was also observed to be lower than the anisotropic samples at both off- and on-state conditions as the higher G’ value in the anisotropic samples had been caused by the existence of chain-like structures in the anisotropic MRE, which had strengthened the interaction between the magnetic particles of the sample. It is important to note that the value of G’ was also influenced by the increasing curing magnetic fields, which had led to stronger formations of chains structures and in turn, a more improved storage modulus. Hence, the increase of G’ can be said to have attributed to the increased stiffness effect on the MRE samples.

In Fig. 8(b), the increment of G’ was observed to be more pronounced at on-state condition since the G’ values for each of the sample were seen to have increased to approximately 50% higher than at off-state settings. The G’ values of the MRE-P samples were also seen to be always higher than those of the MRE-S samples, hence indicating not only a better matrix-particle interaction, but also a stronger interaction between the particles as a result of the larger contact area and the easy magnetization axes of the PL CIPs in the MRE-P samples that had led to a reduction of the inter-particle distance. Meanwhile, the loss factor can be used to evaluate the damping performance of the MRE samples, where it denotes the materials’ ability for dissipating the deformation

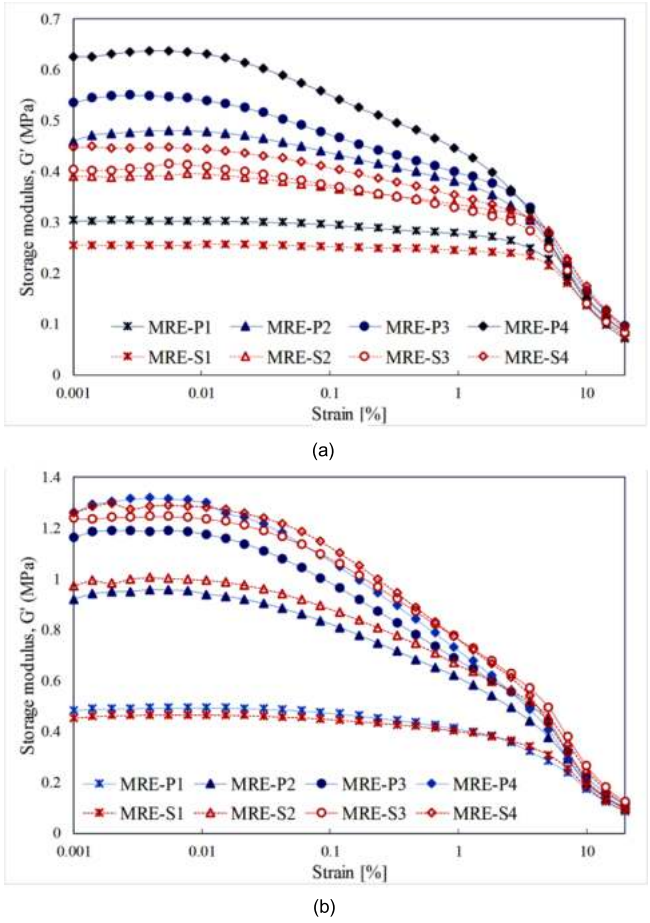

Fig. 7. Strain dependence of storage modulus versus strain at (a) off-state, and (b) on-state conditions.

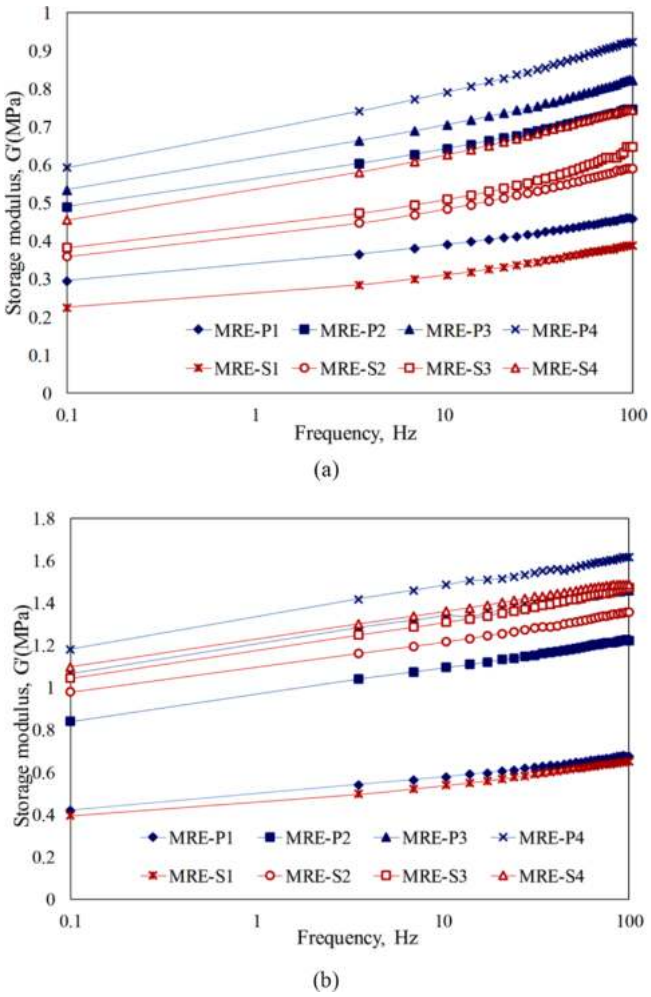

Fig. 8. Frequency dependence of storage modulus at (a) off-state, and (b) on-state conditions with different curing magnetic fields and particle shapes.

Table 3
The summarized value of the initial modulus, G_0, the maximum modulus, G_{max}, and the magneto-induced modulus, ΔG.

	Sample No.	G_0 (off-state) MPa	G_{max} (on-state) MPa	ΔG
1	MRE-S1	0.255	0.451	0.196
2	MRE-S2	0.390	0.972	0.582
3	MRE-S3	0.402	1.238	0.836
4	MRE-S4	0.448	1.259	0.811
5	MRE-P1	0.304	0.481	0.177
6	MRE-P2	0.460	0.918	0.458
7	MRE-P3	0.536	1.162	0.626
8	MRE-P4	0.626	1.261	0.635

energy. Fig. 9 shows the frequency dependence of the loss factor performed at both off- and on-state conditions.

As shown in Fig. 9, the loss factor of both MRE-S and MRE-P samples had shown increasing trends with increasing frequency intensities. While the loss factor for both MRE-S and MRE-P samples were observed to have decreased with increasing curing magnetic fields, the loss factor of the MRE-P samples, however, was seen to be lower than those of the MRE-S samples. In Fig. 9(b), these samples were then subjected to an on-state condition as a way of studying the influence of external magnetic field on the behavior of loss factor. During on-state condition, the loss factor of all the samples had demonstrated lower values than those from the off-state condition. The decrease in the loss factor had therefore proven a lesser heat dissipation under the presence of a magnetic field, which in turn had led to a stronger particle interaction. A larger decrease of the loss factor was observed for anisotropic MRE-P during the on-state condition. The decrease had been due to the smaller frictions of the strongly bounded chain-like structures in the particles, which had indirectly led to the lesser energy dissipation. Meanwhile, another primary source of the loss factor had been the interface interaction between the particles and matrix rather the particle-particle bonding. A weak interface bonding between the particles and matrix will cause an increment of relative motion between the particles and consequently, energy dissipation. As such, higher levels of interactions at interfaces can lead to smaller degrees of loss factor. Conversely, a decrease in the loss factor of the anisotropic samples was also observed with increasing curing magnetic field intensities. This indicates that the chain-like structure had become more complex and had strengthened the interaction force between the particles and the matrix.

Furthermore, by curing the MRE sample under an external magnetic field, the magnetic particles would be inclined to agglomerate in the matrix, hence restraining the matrix. The restrained particle chains would then reduce the friction between the particles and the matrix and as a consequence, decreases the energy dissipation. The loss factor was also found to have decreased with increasing magnetic field intensities. The decrement of the loss factor was most likely due to the increase in the magnetization degree of the particles agglomeration as well as the reduced displacement between the particles as a result of the strong interaction that had linked the particles to the matrix. However, in Fig. 9, it could be observed that the loss factor values had increased steadily with increasing frequency intensities at lower frequencies of 0.1 to 10 Hz with a sudden surge from 10 Hz to 100 Hz, hence attesting

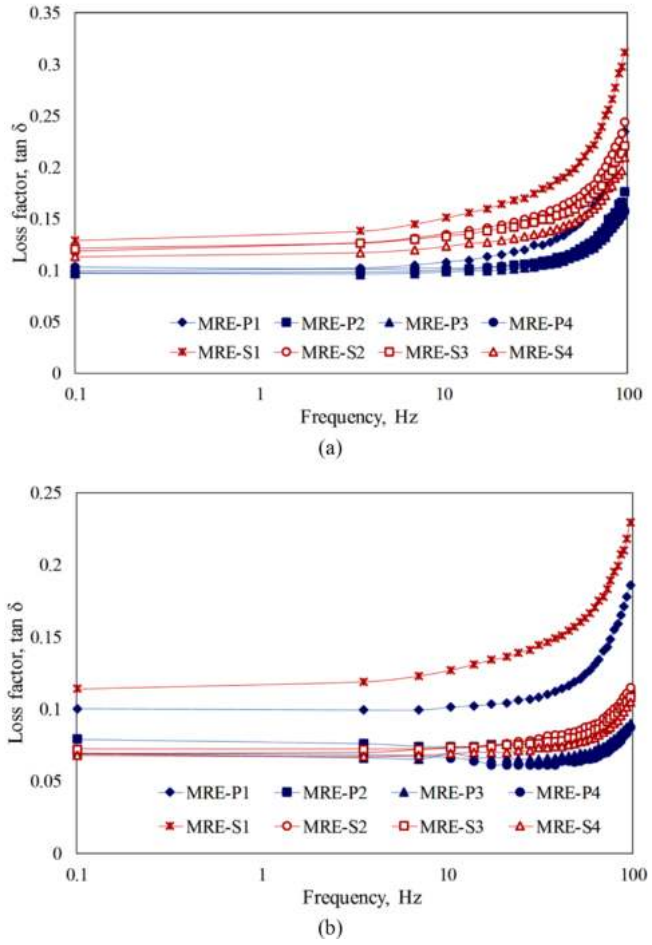

Fig. 9. Frequency dependence of loss factor at (a) off-state, and (b) on-state condition with different curing magnetic fields and particle shapes.

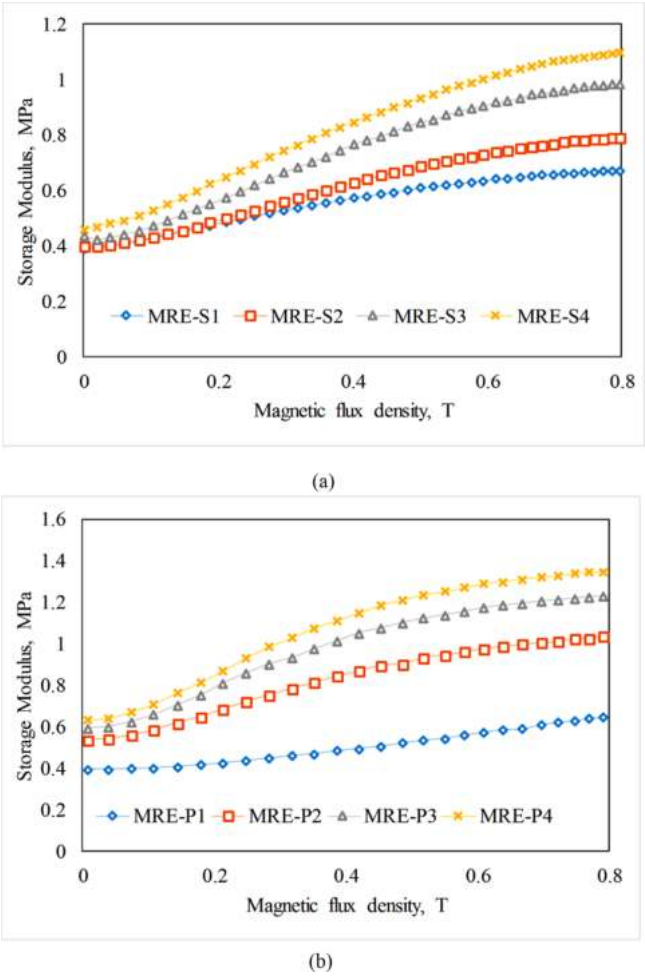

Fig. 10. The shear storage modulus of MRE with different curing current examined on the various magnetic flux density (a) MRE-S, (b) MRE-P.

to the fact that the MRE samples loss factor indeed has a frequency dependence trait. The increase in the loss factor was also attributed to the improved interfacial slippage via higher energy dissipation caused by the high-frequency intensities.

An analysis on the effects of particle shapes on the loss factor was also conducted. As shown in Fig. 9(a) and (b), the loss factor for MRE-P was observed to be lower than that of the MRE-S samples with or without the presence of a testing magnetic field, as demonstrated by the decline of the lowest loss factor value in the MRE-P4 sample from 0.097 at off-state to 0.068 in an on-state condition. As for the MRE-S4 sample, the loss factor at off-state condition was 0.113 and had declined to 0.068 in an on-state condition. The lower loss factor value in the MRE-P samples had therefore implied a lesser energy dissipation of the interfacial slippage between the particles and matrix. It is well-known that the main factor contributing to the damping property of the MRE would be that of a matrix-particle interaction rather than a particle-particle interaction. As such, for the case of the MRE-P samples, the milling process had resulted not only increases in the diameter and the surface contact areas but had also led to an increased interaction between the matrix and particles. This result had agreed well with the micrograph analysis shown in Fig. 6(d), where the distances between the particles were shown to have reduced and led to the interface slippage resilience of the matrix and particles. Hence, this analysis had proven that a strong interaction between the matrix and the particles would lead to lesser energy dissipation in the system and decrements of the loss factor.

Magnetic field sweep test

The shearing test of the MRE under the presence of an external magnetic field would cause the magnetic particles (CIP) in the matrix materials to be magnetized as a result of the dipole-dipole interactions between the particles. An additional effort is then required for these magnetic particles to vibrate from their minimum energy state, hence giving rise to a field-dependent shear modulus. Furthermore, these magnetic particles would have a tendency to align according to the direction of the magnetic field as well as restrict the deformation of the matrix, thus resulting in changes of the modulus. The key parameter for evaluating the relative change of modulus is known as MR effect, which can be expressed by the following equation:

$$G_{MRE}(\%) = \frac{(G_{max} - G_0)}{G_0} \times 100\%$$

where G_0 is the initial storage modulus and G_{max} is the maximum shear storage modulus under the presence of a magnetic field. The respective shear storage modulus and relative MR effect under different magnetic fields for MRE samples with various CIPs shapes (MRE-S and MRE-P) are shown in Fig. 10.

As shown in Fig. 10, all the samples had exhibited MR effects behaviour, where the G' for all the MRE samples were observed to have increased steadily with increasing testing magnetic flux densities. The initial and magneto-induced moduli as well as the relative MR effects for all the MRE samples are summarized in Table 4.

In Table 4, while the isotropic MRE-S1 and MRE-P1 had shown a

Table 4
Summarized of magnetorheological properties of MRE samples.

Samples	G_o (MPa)	ΔG_{max} (MPa)	Relative MR effect (%)
MRE-S1	0.39189	0.28564	73
MRE-P1	0.39652	0.28226	71
MRE-S2	0.40124	0.39076	97
MRE-P2	0.53804	0.50566	94
MRE-S3	0.43461	0.54594	125
MRE-P3	0.59367	0.65023	109
MRE-S4	0.45896	0.63254	137
MRE-P4	0.63394	0.72436	114

negligible increment in the relative MR effect, all of the anisotropic MREs on the other hand, had demonstrated otherwise. The G_0 of the isotropic samples were also observed to be lower than those of the anisotropic samples, as shown by the G_0 for the isotropic samples, MRE-S1 and MRE-P1, which had a respective lowest value of 0.392 MPa and 0.396 MPa. In terms of the MR effects, the percentage had been lowered for the isotropic MRE-S1 and MRE-P samples with a corresponding 73 and 71%, as opposed to those of anisotropic MREs (MRE-S4, and MRE-P4), where it had achieved up to 137 and 114% during a curing at 345 mT. It is a well-known fact that the interactions between the particles would become stronger under anisotropic conditions because of the chain-like structures formation during the curing process. The influence of external magnetic field will increase the initial modulus of the anisotropic MREs as a result of the higher restrained rubber being entrapped within the CIPs. This will then lead to a higher resistance level of the magnetic particles toward the deformation of shear directions during dynamic testing. In the case of isotropic MREs however, the low initial modulus was mainly attributed to the random distribution arrangement of CIPs and the unrestricted matrix between the CIPs.

Although the G_0 in both anisotropic MRE-S and MRE-P samples were seen to have increased with increasing curing magnetic fields, the G_0 value for the anisotropic MRE-P was found to be higher than those of the anisotropic MRE-S with the same CIP content. These results had therefore shown samples that were cured under strong curing magnetic field to have a greater MR effect. The MR effect in this case, had strongly depended on the strength of the magnetic field since a higher magnetic field would lead to a reduced distance between the magnetic particles and result in a stronger bonding interaction of magnetic particles in the MRE samples. This phenomenon had therefore explained the greater MR effect of the anisotropic MREs, which had agreed well with the previous studies conducted by other researchers [16, 48]. However, as listed in Table 4, the relative MR effect of the MRE-P samples for both isotropic and anisotropic types was found to be lower than those of the MRE-S, which could be explained by the higher initial modulus exhibited by the MRE-P. Obviously, this result had not only proven the MRE-P sample to be much stiffer than the MRE-S, but had also implied a lesser MRE-P deformation under increasing curing current intensities. The higher initial modulus for MRE-P as shown by the increase of 0.396–0.634 MPa during curing, is believed to have occurred as a result of the higher density and a more compact structure of PL CIPs as well as the higher aspect ratio caused by the increased average diameter shown in Fig. 6(c) and (d). Although the minimal influence of MRE-P on the relative MR effect had appeared to be attributed to the shapes of the particles, the phenomenon can also be explained by the stacking orientation of the PL CIPs inside the rubber matrix, where the chain-like structures of PL CIPs may have formed magnetic clusters in the matrix, hence increasing the restrained rubber that was trapped within the particles and reduces the distances between the particles.

Conclusions

In this study, two types of MRE (MRE-S and MRE-P) were successfully prepared from the PL-CIPs that were modified from SL-CIPs via a ball milling technique. Apart from the morphologies, phase characterization and magnetic properties, the rheological properties effect towards the different shapes of CIPs and the strength of curing magnetic field of the two MRE samples were also experimentally investigated and discussed in detail. Although the milling process was found to have not affected the structural characterization of the CIPs, the analysis of its magnetic properties however, had shown the magnetic saturation of PL-CIPs to have declined to 141.39 emu/g because of the oxidation that had occurred during the milling process. The field-dependent modulus of MRE-P was found to be higher than those of the MRE-S, hence implying the lower MR effect of the MRE-P to be attributed by the higher initial stiffness level. The highest MRE effect achieved by MRE-P (MRE-P4) was 114%, while the MRE-S (MRE-S4) had attained 135%. The damping property of the MRE-P samples was also observed to be lower than those of the MRE-S as a result of the strong matrix-particle interaction that had led to lesser energy dissipation during the deformation process. In conclusion, the findings gained from this study are seen as useful and can be considered in the future studies of the MRE field.

Acknowledgment

This work is supported and funded by Professional Development Research University (PDRU) grant (Vot No. 04E02). Authors also acknowledge partial support from USAID through Sustainable Higher Education Research Alliances (SHERA) Program - Centre for Collaborative (CCR) National Center for Sustainable Transportation Technology (NCSTT) with Contract No. IIE00000078-ITB-1 as well as Universitas Sebelas Maret through Hibah Perkuatan Kapasitas Laboratorium (PKLP) 2019.

Appendix A. Supplementary material

Supplementary data to this article can be found online at https://doi.org/10.1016/j.rinp.2019.02.045.

References

[1] Yu M, Fu J, Ju BX, Zheng X, Choi SB. Influence of x-ray radiation on the properties of magnetorheological elastomers. Smart Mater Struct 2013;22:125010.
[2] Balasoiu M, Bica I. Results in physics composite magnetorheological elastomers as dielectrics for plane capacitors: effects of magnetic field intensity. Results Phys 2016;6:199–202.
[3] Qi S, Yu M, Fu J, Li PD, Zhu M. Creep and recovery behaviors of magnetorheological elastomer based on polyurethane/epoxy resin IPNs matrix. Smart Mater Struct 2016;25:015020.
[4] Lokander M, Stenberg B. Improving the magnetorheological effect in isotropic magnetorheological rubber materials. Polym Test 2003;22:677–80.
[5] Farshad M, Benine A. Magnetoactive elastomer composites. Polym Test 2004;23:347–53.
[6] Li WH, Nakano M. Fabrication and characterization of PDMS based magnetorheological elastomers. Smart Mater Struct 2013;22:055035.
[7] Ju B, Tang R, Zhang D, Yang B, Yu M, Liao C, et al. Dynamic mechanical properties of magnetorheological elastomers based on polyurethane matrix. Polym Compos 2016;37:1587–95.
[8] Deng H-X, Gong X-L. Application of magnetorheological elastomer to vibration absorber. Commun Nonlinear Sci Numer Simul 2008;13:1938–47.
[9] Kim HK, Kim HS, Kim Y-K. Stiffness control of magnetorheological gels for adaptive tunable vibration absorber. Smart Mater Struct 2017;26:015016.
[10] Koo J-H, Dawson A, Jung H-J. Characterization of actuation properties of magnetorheological elastomers with embedded hard magnetic particles. J Intell Mater Syst Struct 2012;23:1049–54.
[11] Böse H, Rabindranath R, Ehrlich J, Bo H, Böse H, Rabindranath R, et al. Soft magnetorheological elastomers as new actuators for valves. J Intell Mater Syst Struct 2012;23:989–94.
[12] Liao GJ, Gong X, Xuan SH, Kang CJ, Zong LH. Development of a real-time tunable stiffness and damping vibration isolator based on magnetorheological elastomer. J Intell Mater Syst Struct 2012.
[13] Abramchuk S, Kramarenko E, Stepanov G, Nikitin LV, Filipcsei G, Khokhlov AR, et al. Novel highly elastic magnetic materials for dampers and seals: Part I. Preparation and characterization of the elastic materials. Polym Adv Technol 2007;18:883–90.
[14] Li W, Kostidis K, Zhang X, Zhou Y, Zhang Xianzhou, Zhou Yang, et al. Development

of a force sensor working with MR elastomers. 2009 IEEE/ASME Int. Conf. Adv. Intell. Mechatronics, IEEE 2009:233–8.
[15] Li WH, Tian TF, Du H. Smart actuation and sensing systems – recent advances and future challenges. InTech 2012.
[16] Bunoiu M, Bica I. Magnetorheological elastomer based on silicone rubber, carbonyl iron and Rochelle salt: Effects of alternating electric and static magnetic fields intensities. J Ind Eng Chem 2015;37:1–7.
[17] Palacios-pineda LM, Perales-martinez IA, Lozano-sanchez LM, Mart O, Segura-c E. Magnetorheological behavior of PDMS elastomer reinforced with iron micro/nanoparticles. Polymers 2017.
[18] Park SH, Bandaru PR. Improved mechanical properties of carbon nanotube/polymer composites through the use of carboxyl-epoxide functional group linkages. Polymer (Guildf) 2010;51:5071–7.
[19] Kumar V, Lee D. Iron particle and anisotropic effects on mechanical properties of magneto-sensitive elastomers. J Magn Magn Mater 2017;441:105–12.
[20] Tong Y, Dong X, Qi M. Improved tunable range of the field-induced storage modulus by using flower-like particles as the active phase of magnetorheological elastomers. Soft Matter 2018;14:3504–9.
[21] Upadhyay RV, Laherisheth Z, Shah K. Rheological properties of soft magnetic flake shaped iron particle based magnetorheological fluid in dynamic mode. Smart Mater Struct 2014;23:015002.
[22] Jahan N, Pathak S, Jain K, Pant RP. Enchancement in viscoelastic properties of flake-shaped iron based magnetorheological fluid using ferrofluid. Colloids Surf A Physicochem Eng Asp 2017;529:88–94.
[23] Shah K, Phu DX, Seong M-S, Upadhyay RV, Choi S-B. A low sedimentation magnetorheological fluid based on plate-like iron particles, and verification using a damper test. Smart Mater Struct 2014;23:027001.
[24] Shah K, Choi S. The influence of particle size on the rheological properties of plate-like iron particle based magnetorheological fluids. Smart Mater Struct 2015;24:015004.
[25] Shilan ST, Mazlan SA, Ido Y, Hajalilou A, Jeyadevan B, Choi S-B, et al. A comparison of field-dependent rheological properties between spherical and plate-like carbonyl iron particles-based magneto-rheological fluids. Smart Mater Struct 2016;25:095025.
[26] Mohamad N, Mazlan SA, Imaduddin F, Choi S-B, Yazid IIM. A comparative work on the magnetic field- dependent properties of plate-like and spherical iron particle-based magnetorheological grease. PLoS One 2018;13:1–16.
[27] Zheng D, Liu T, Zhou L, Xu Y. Electromagnetic absorbing property of the flaky carbonyl iron particles by chemical corrosion process. J Magn Magn Mater 2016;419:119–24.
[28] Han R, Qiao L, Wang T, Li F. Microwave complex permeability of planar anisotropy carbonyl-iron particles. J Alloys Compd 2011;509:2734–7.
[29] Song Z, Xie J, Zhou P, Wang X, Liu T, Deng L. Toughened polymer composites with flake carbonyl iron powders and their electromagnetic/absorption properties. J Alloys Compd 2013;551:677–81.
[30] Kong LB, Li ZW, Liu L, Huang R, Abshinova M, Yang ZH, et al. Recent progress in some composite materials and structures for specific electromagnetic applications. Int Mater Rev 2013;58:203–59.
[31] Bell RC, Miller ED, Karli JO, Vavreck AN, Zimmerman DT. Influence of particle shape on the properties of magnetorheological fluids. Int J Mod Phys B 2007;21:5018–25.
[32] Qiao L, Wen F, Wei J, Wang J, Li F. Microwave permeability spectra of flake-shaped FeCuNbSiB particle composites. J Appl Phys 2008;103:1–6.
[33] Boczkowska A, Awietjan SF, Wroblewski R. Microstructure–property relationships of urethane magnetorheological elastomers. Smart Mater Struct 2007;16:1924–30.
[34] Fan Y, Gong X, Xuan S, Zhang W, Zheng J, Jiang W. Interfacial friction damping properties in magnetorheological elastomers. Smart Mater Struct 2011;20:035007.
[35] Gong X, Zhang XZ, Zhang PQ. Study of mechanical behavior and microstructures of magnetorheological elastomers. Int J Mod Phys B 2005;19:1304–10.
[36] Fan YC, Gong XL, Jiang WQ, Zhang W, Wei B, Li WH. Effect of maleic anhydride on the damping property of magnetorheological elastomers. Smart Mater Struct 2010;19:055015.